Supporting Information

Efficient Photoinduced Energy and Electron Transfers in a Tetraphenylethene-Based Octacationic Cage through Host-Guest Complexation

Honghong Duan,[1] Fan Cao,[1] Hongxing Hao,[2] Hongtao Bian,[2] and Liping Cao[1,*]

[1]College of Chemistry and Materials Science, Northwest University, Xi'an, 710069, P. R. China.

[2]Key Laboratory of Applied Surface and Colloid Chemistry of Ministry of Education, School of Chemistry and Chemical Engineering, Shaanxi Normal University, Xi'an 710062, P. R. China.

[*]e-mail: chcaoliping@nwu.edu.cn

Table of Contents **Pages**

Experimental Procedures

General Experimental Details.

Starting materials were purchased from commercial suppliers were used without further purification. NMR spectra were recorded on a spectrometer operating at 400 MHz for ^{1}H NMR spectra on a Bruker ascend spectrometer. UV/vis spectra were done on Agilent Cary-100 spectrometer. Fluorescence spectra were performed by using a Horiba Fluorolog-3 spectrometer and the absolute photoluminescence quantum efficiency were acquired by using an integrating sphere. Fluorescence decay profiles were recorded on a Flsp920. The CV measurement was conducted in dimethylsulfoxide (DMSO) with 0.1 M tetrabutylammonium hexafluorophosphate as the supporting electrolyte at a scan rate of 50 mV s^{-1}, using platinum as the working electrode, saturated calomel electrode (SCE) as the reference electrode, and platinum wire counter electrode. The SCE reference electrode was calibrated using the ferrocene/ferrocenium (Fc/Fc+) redox couple as an external standard. The fsTA measurements were performed based on a femtosecond Ti:Sapphire regenerative amplified Ti:sapphire laser system (Spectra Physics, Spitfire-Pro) and an automated data acquisition system (Ultrafast Systems, Helios model).

Materials.

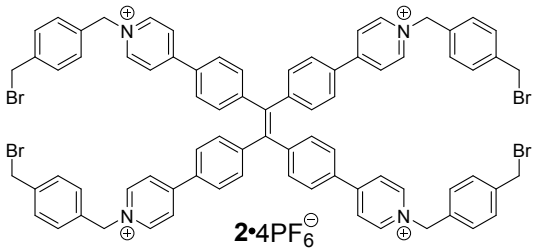

Nile Red (**NiR**), Rhodamine 700 (**R700**), Rhodamine 800 (**R800**), Indocyanine Green (**ICG**), Acid Green 25 (**AG**), Acid Violet 43 (**AV**), and other materials/solvents were purchased and used as received. **1**•8PF_6^-, **1**•8Cl^-, and **2**•4PF_6^- were synthesized by previously reported procedures.[1]

NMR experiment

^{1}H NMR spectra were recorded on a Bruker ascend spectrometer. Chemical Shifts are recorded in ppm (δ) in D_2O (internal reference set to δ 4.79), CD_3CN (internal reference set to δ 2.13). Titrations were performed by using stock solutions of host and guest to make up samples of desired concentrations and equivalents. All spectra were recorded at 298 K.

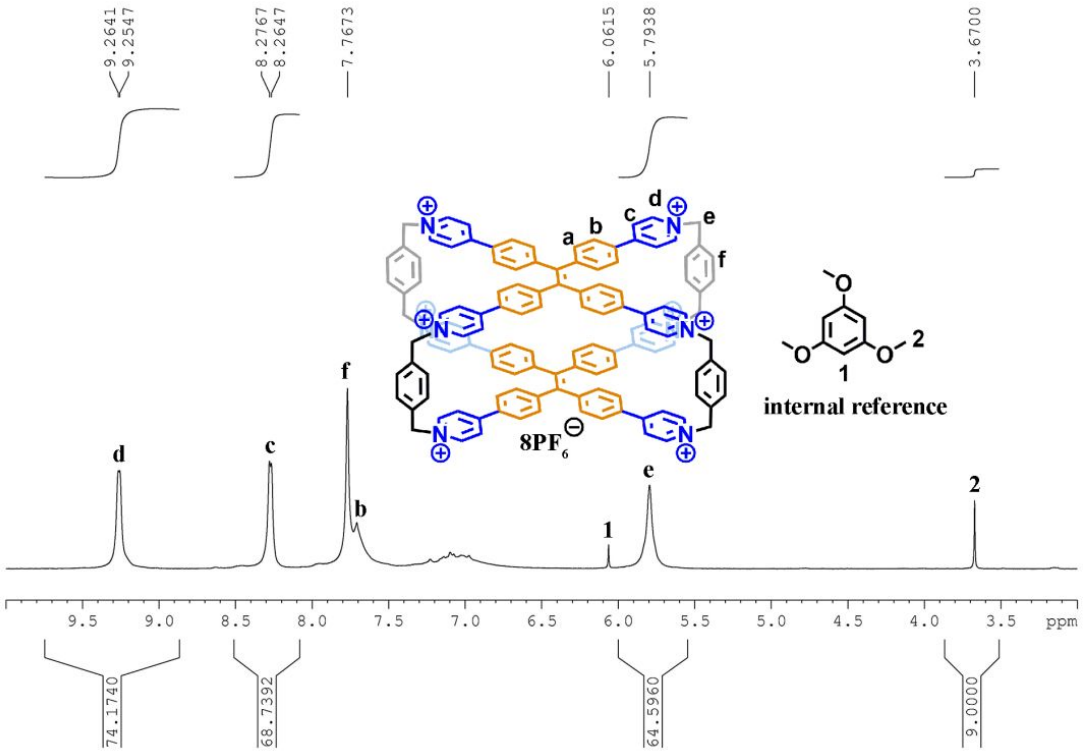

Figure S1. ^{1}H NMR (400 MHz, DMSO-d_6) of **1** (20 μL saturated solution of **1** in CD_3CN was dried in high vacuum) with 20 μL of 1,3,5-trimethoxy-benzen (20.0 mM) as internal reference. The solubility of **1** was calculated as 86.4 mM based on the average integral from three proton resonances (H_d, H_c, and H_e).

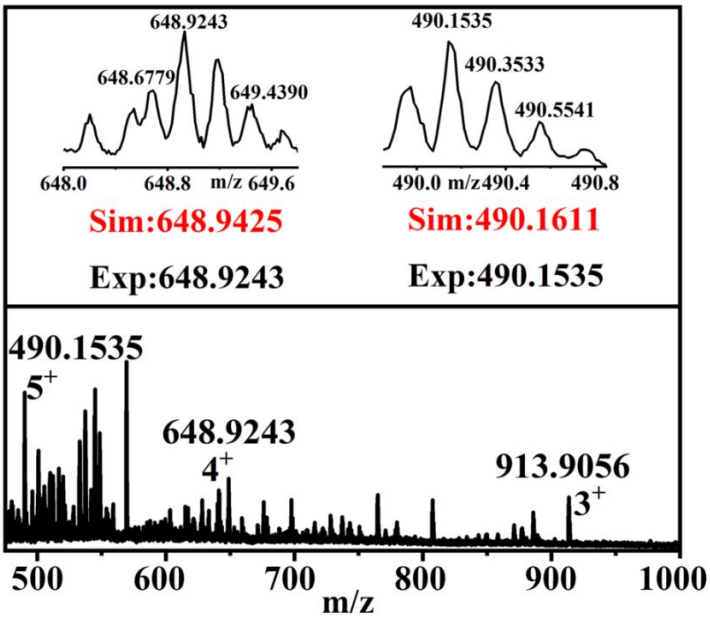

Figure S2. Experimental and calculated electrospray ionization mass spectra of **1**•8PF_6^- □**NiR**.

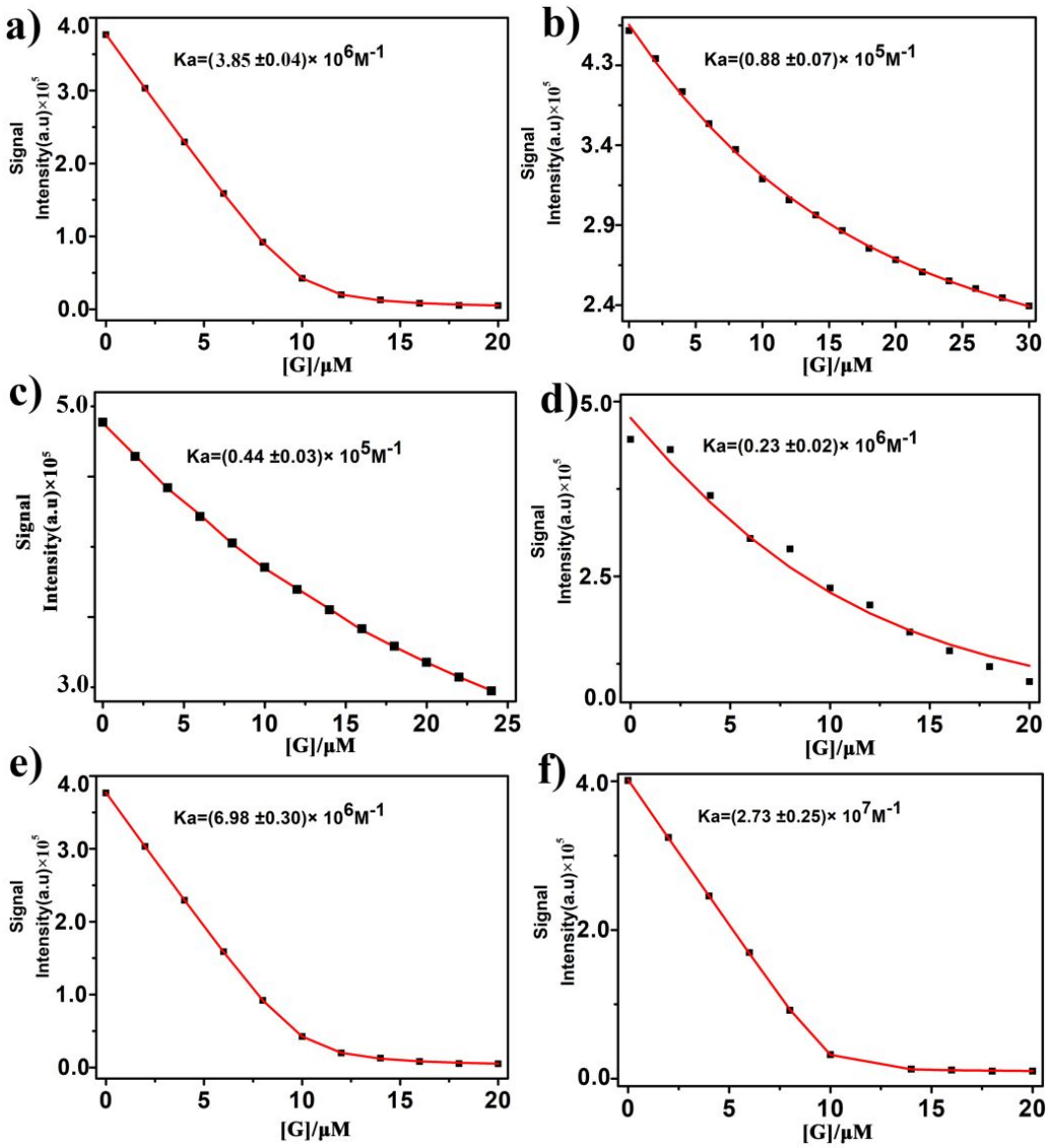

Figure S3. The calculation of the host-guest binding constant was fitted with dynifit by the data of fluorescence titration. a) **1**•8PF_6^- and **NiR** in CH_3CN; b) **1**•8Cl^- and **R700**; c) **1**•8Cl^- and **R800**; d) **1**•8Cl^- and **ICG**; e) **1**•8Cl^- and **AG**; f) **1**•8Cl^- and **AV** in H_2O.

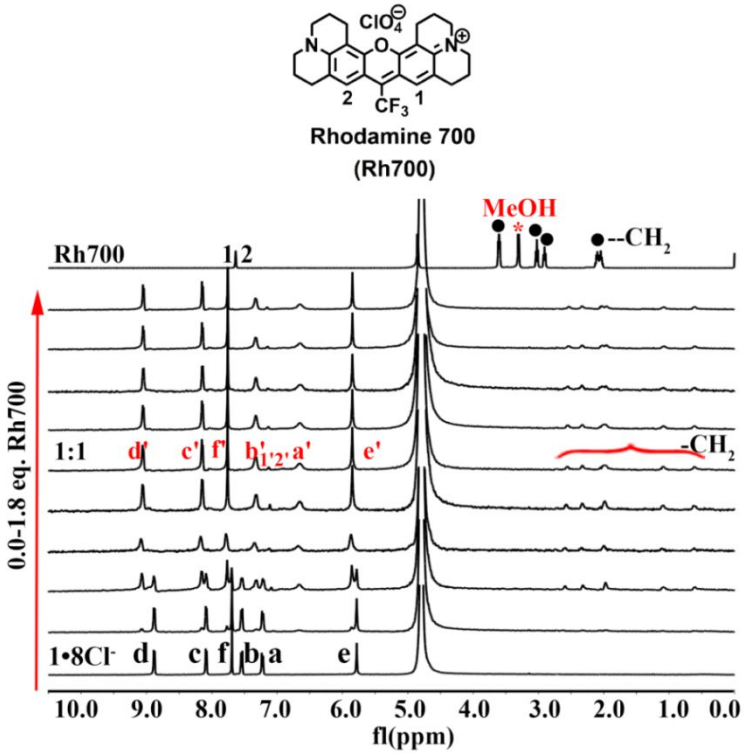

Figure S4. ^{1}H NMR titration (400 MHz, D_2O, RT) **1**•8Cl$^-$ (0.40 mM) titrated with **R700** (0−2.0 equiv).

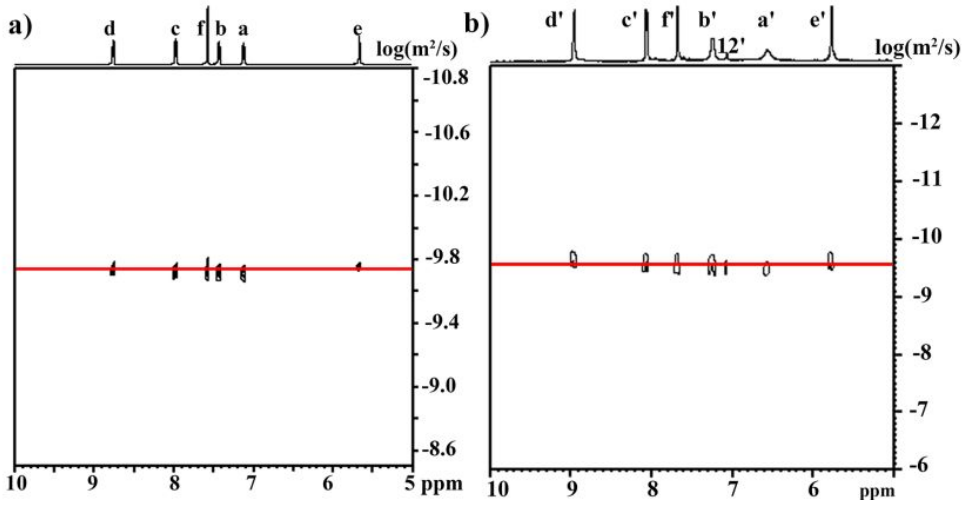

Figure S5. DOSY spectra recorded (400 MHz, D_2O, RT) for (a) **1**•8Cl$^-$ and (b) **1**•8Cl$^-$ □**R700**.

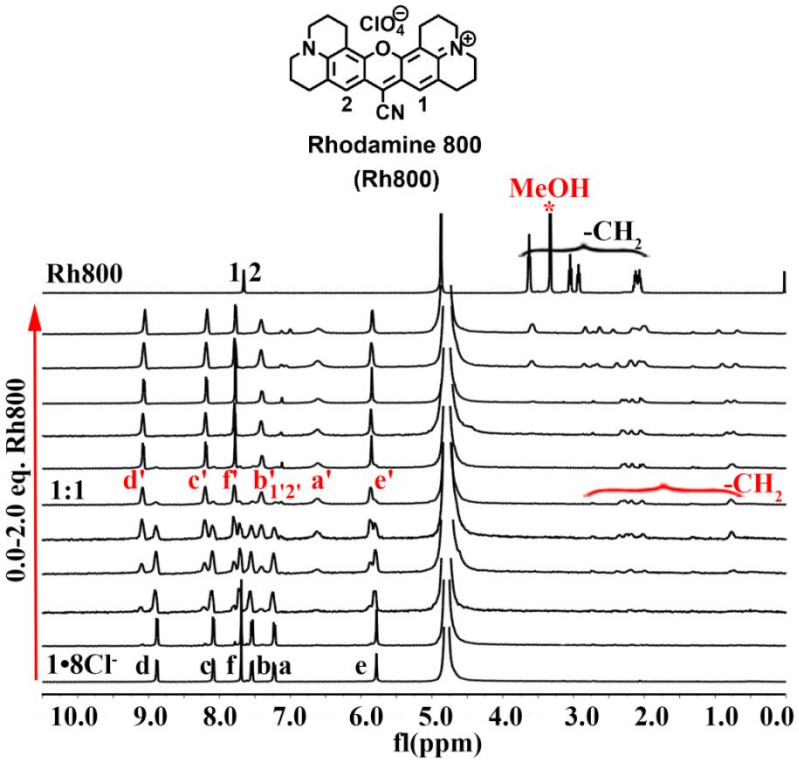

Figure S6. ^{1}H NMR titration (400 MHz, D_2O, RT) **1**•8Cl$^-$ (0.40 mM) titrated with **R800** (0−2.0 equiv).

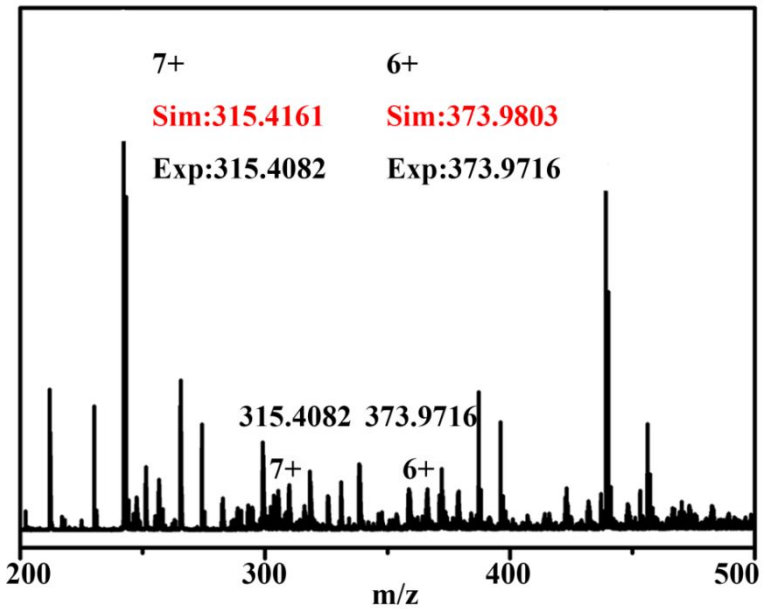

Figure S7. Experimental and calculated electrospray ionization mass spectra of **1**•8Cl$^-$ □**R700**.

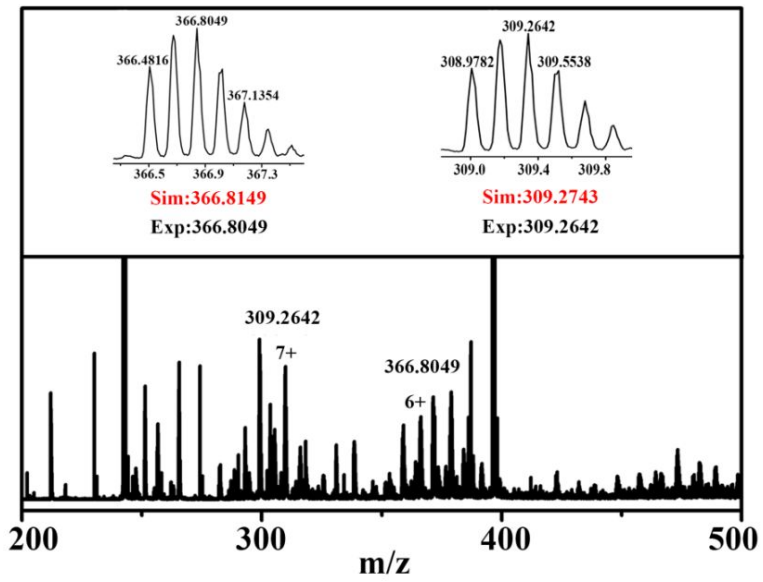

Figure S8. Experimental and calculated electrospray ionization mass spectra of **1**•8Cl$^-$ □**R800**.

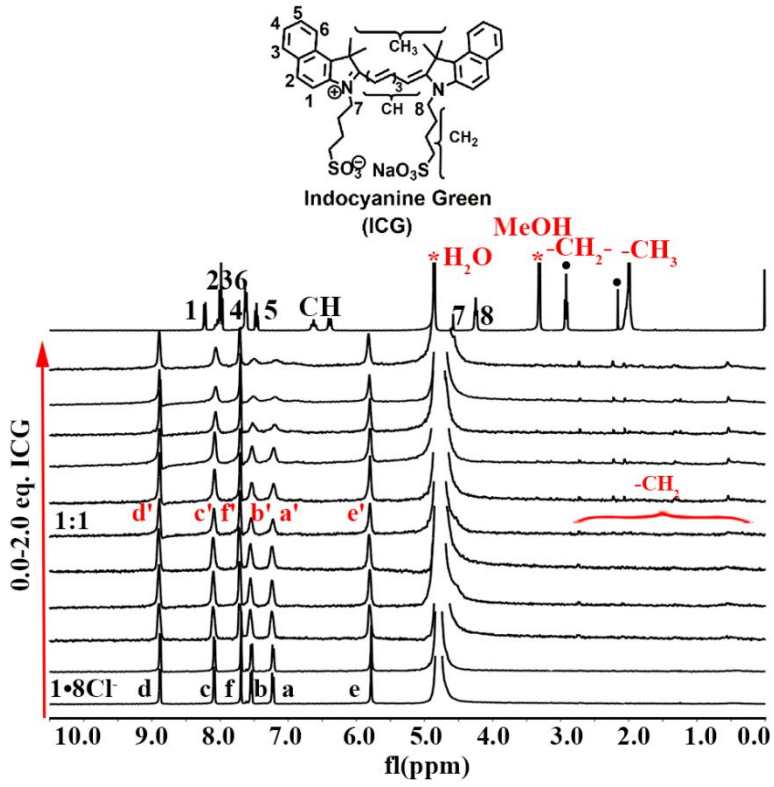

Figure S9. ^{1}H NMR titration (400 MHz, D_2O, RT) **1**•8Cl$^-$ (0.40 mM) titrated with **ICG** (0−2.0 equiv).

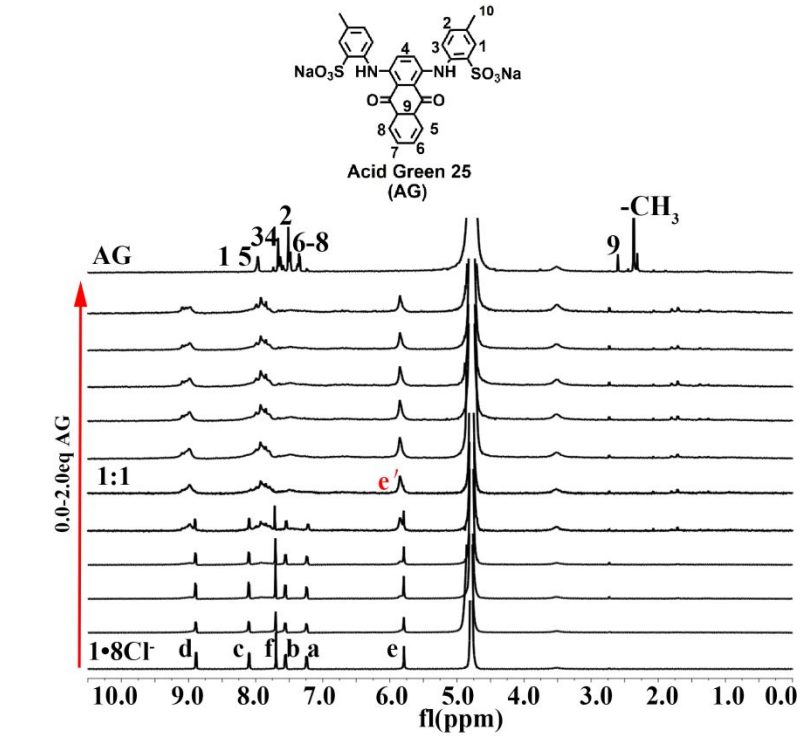

Figure S10. ^{1}H NMR titration (400 MHz, D_2O, RT) **1**•8Cl$^-$ (0.40 mM) titrated with **AG** (0−2.0 equiv).

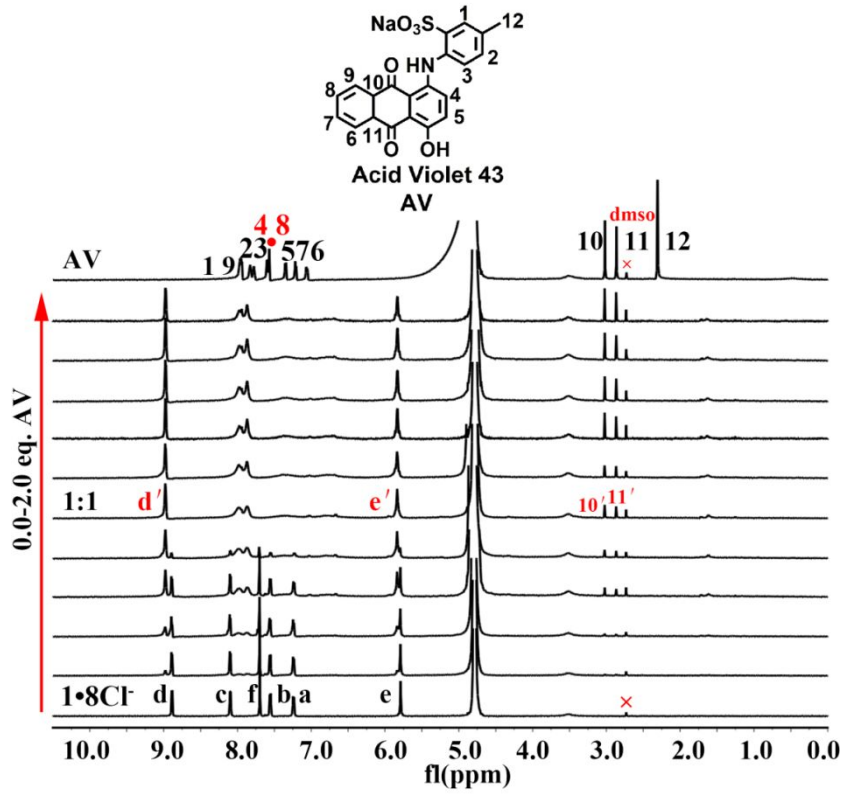

Figure S11. ^{1}H NMR titration (400 MHz, D_2O, RT) **1**•8Cl$^-$ (0.4 mM) titrated with **AV** (0−2.0 equiv.).

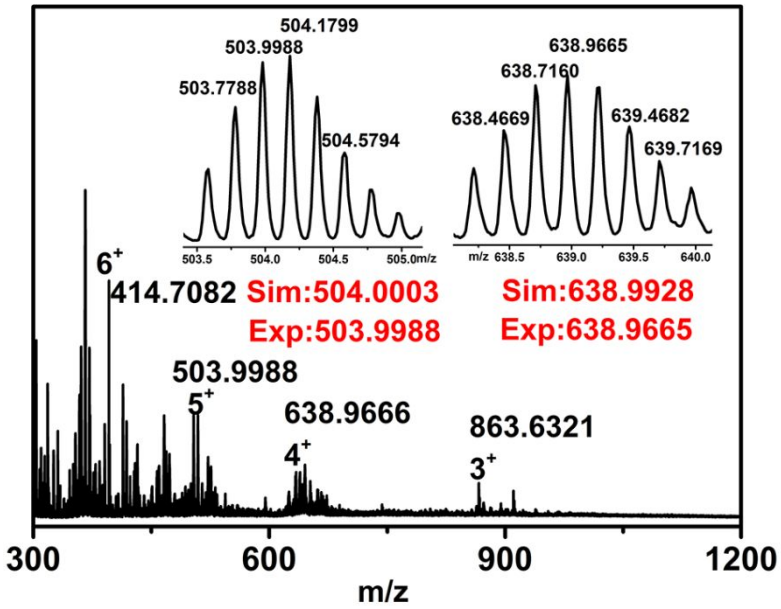

Figure S12. Experimental and calculated electrospray ionization mass spectra of **1**•8Cl$^-$□**ICG**.

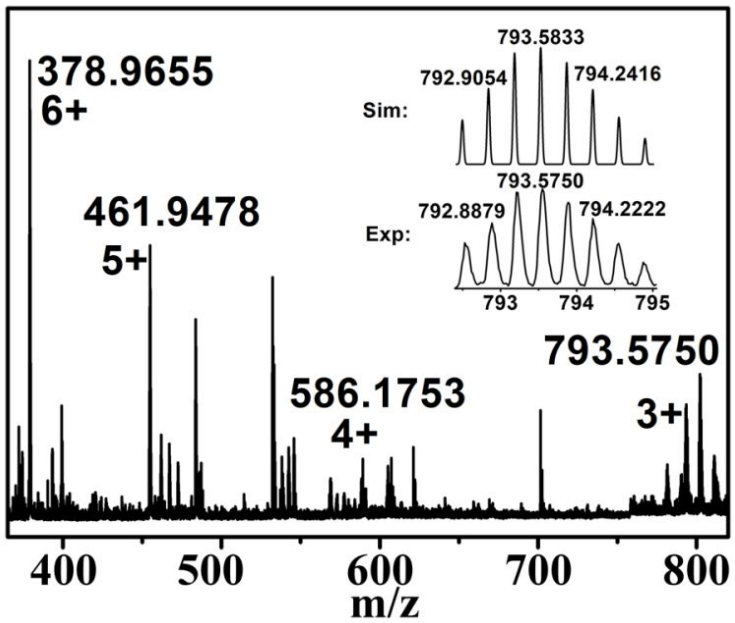

Figure S13. Experimental and calculated electrospray ionization mass spectra of **1**•8Cl$^-$□**AG**.

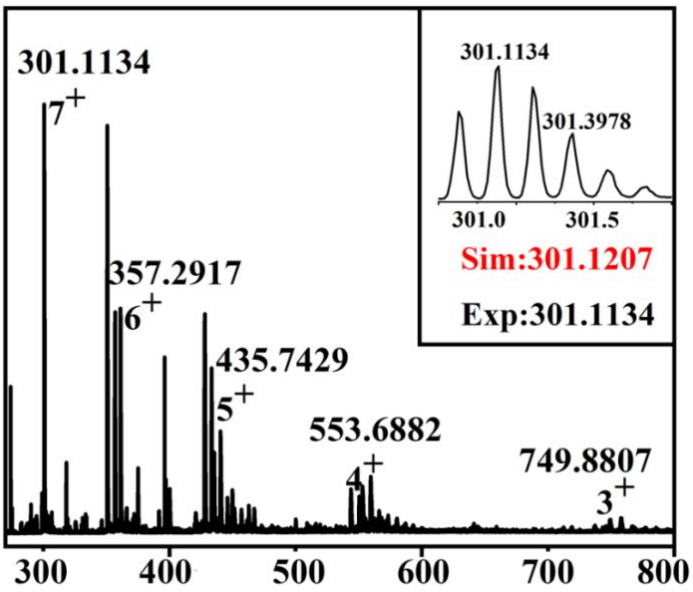

Figure S14. Experimental and calculated electrospray ionization mass spectra of **1**•8Cl$^-$ □**AV**.

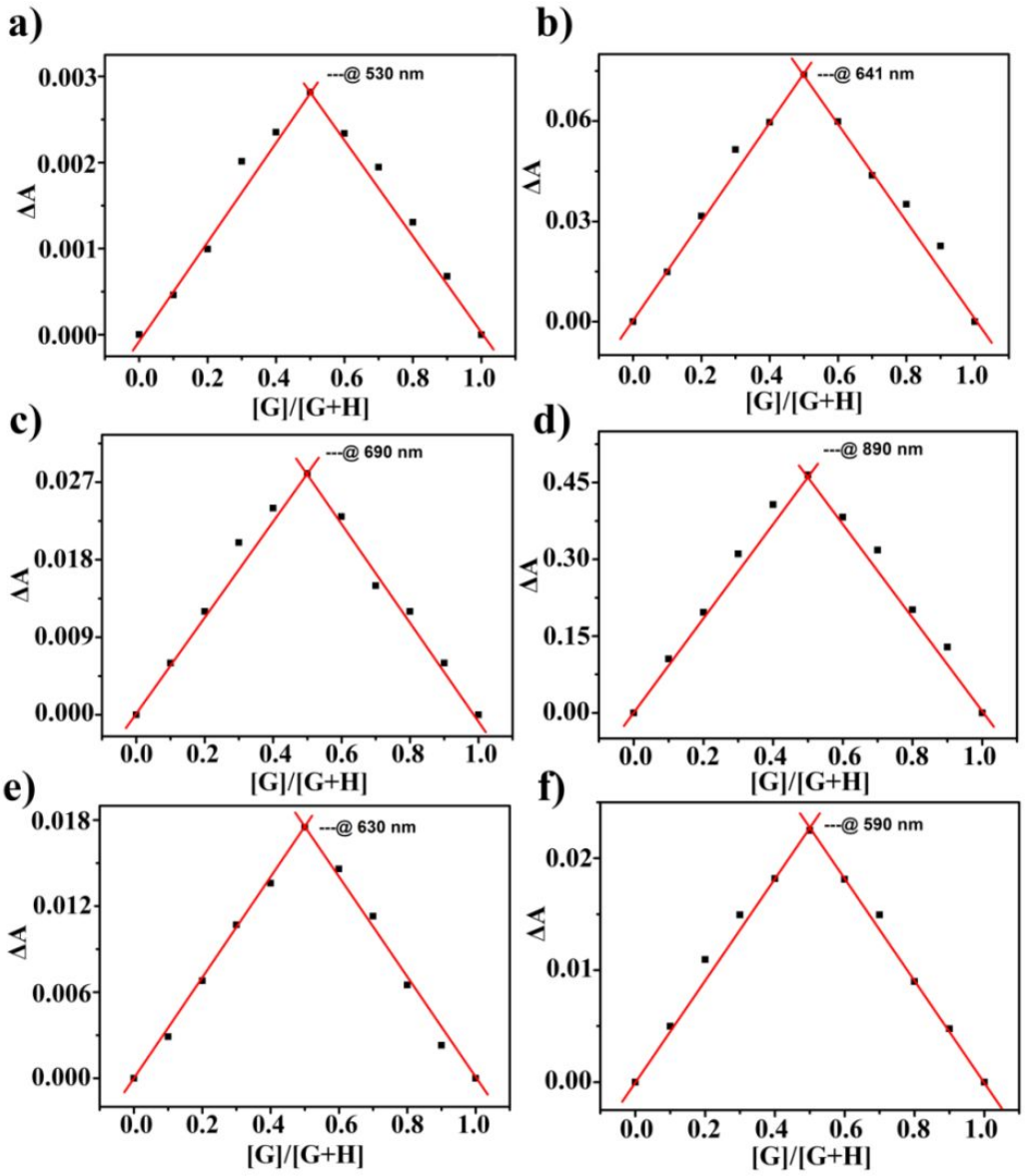

Figure S15. Job plot for the host-guest complexes between cage and dyes guest at room temperature, showing a 1:1 binding in solution: a) **1**•8PF_6^- and **NiR** in CH_3CN; b) **1**•8Cl^- and **R700**; c) **1**•8Cl^- and **R800**; d) **1**•8Cl^- and **ICG**; e) **1**•8Cl^- and **AG**; f) **1**•8Cl^- and **AV** in H_2O.

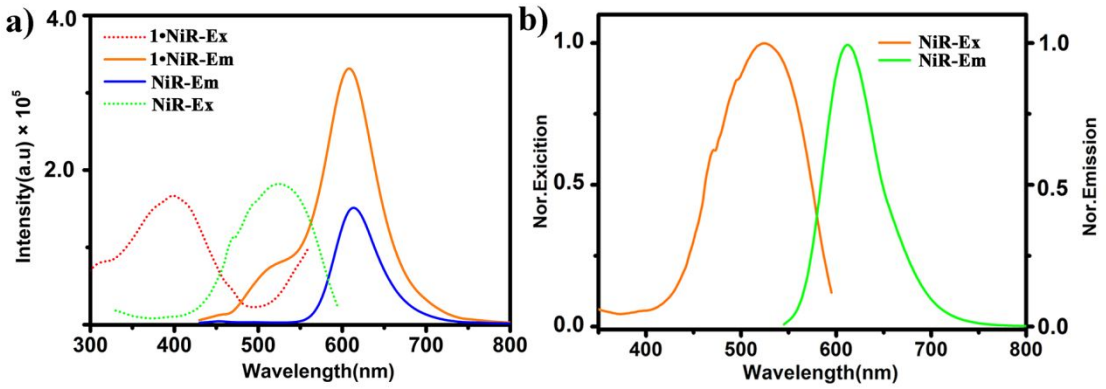

Figure S16. (a) Excitation and emission spectra of **NiR** and **1**•8PF_6^- **NiR** in CH_3CN. Ex/Em slit = 1.6 nm, λ_{ex} = 410 nm. (b) Normalized fluorescence excitation and emission spectra of **NiR**.

Table S1. Fluorescence quantum yield and Fluorescence lifetime of dyes

Compound	Fluorescence quantum yield	Fluorescence lifetime
	Φ_F (%)	τ_F (ns)[c,d]
NiR	41.16[a]	4.86
R700	0.20[b]	5.70
R800	0.79[b]	5.76
ICG	0.1[b]	–
AG	0.55[b]	–
AV	0.1[b]	–

[a]Determined in CH_3CN (10 μM); [b]Determined in water (10 μM); [c]Average lifetimes $\tau = \{(A_1\tau_1 + A_2\tau_2)/100\}$; [d]Decay at 545 nm; [f]Decay at 610 nm (**NiR**), 680 nm (**R700**), 715 nm (**R800**), respectively.

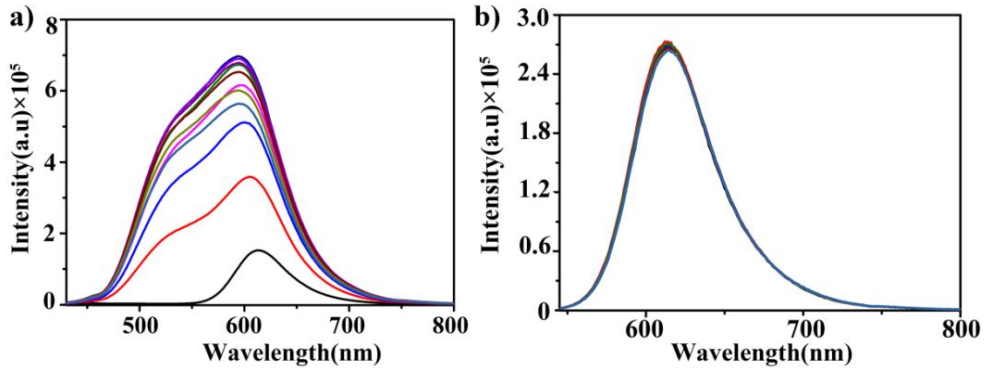

Figure S17. Fluorescence spectra of **NiR** (10 μM) titrated with **1**•8PF_6^- (0−2.0 equiv) in CH_3CN: (a) λ_{ex} = 410 nm, (b) λ_{ex} = 525 nm. Ex/Em slit = 1.6 nm.

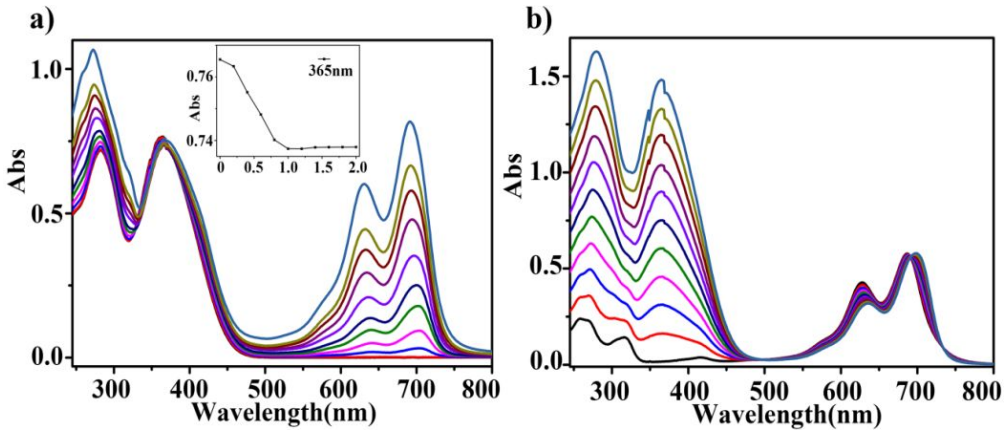

Figure S18. (a) UV/vis spectra of **1**•8Cl^- (10 μM) titrated with **R800** (0−3.0 equiv) in H_2O. (b) UV/vis spectra of **R800** (10 μM) titrated with **1**•8Cl^- (0−2.0 equiv) in H_2O.

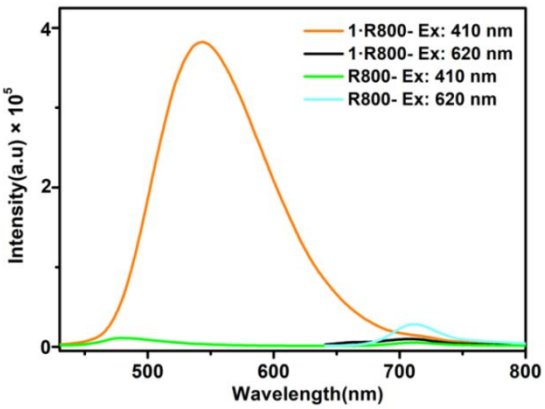

Figure S19. Fluorescence spectra of fluorescence spectra of **1**•8Cl^-□**R800** (10 μM) and **R800** (10 μM) upon different excitation. Ex/Em slit = 1.6 nm, λ_{ex} = 410/620 nm.

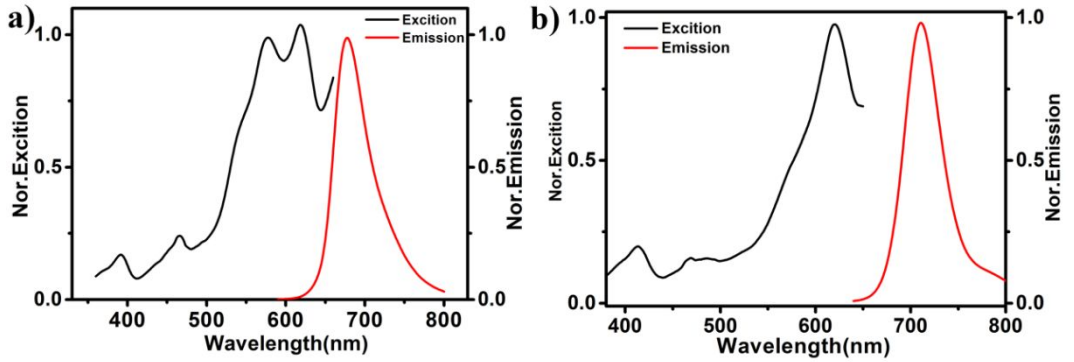

Figure S20. Normalized fluorescence excitation (black) and emission (red) spectra of (a) **R700** and (b) **R800** in H_2O. Ex/Em slit = 1.5 nm, [**R700**] = [**R800**] = 1.0×10^{-5} M.

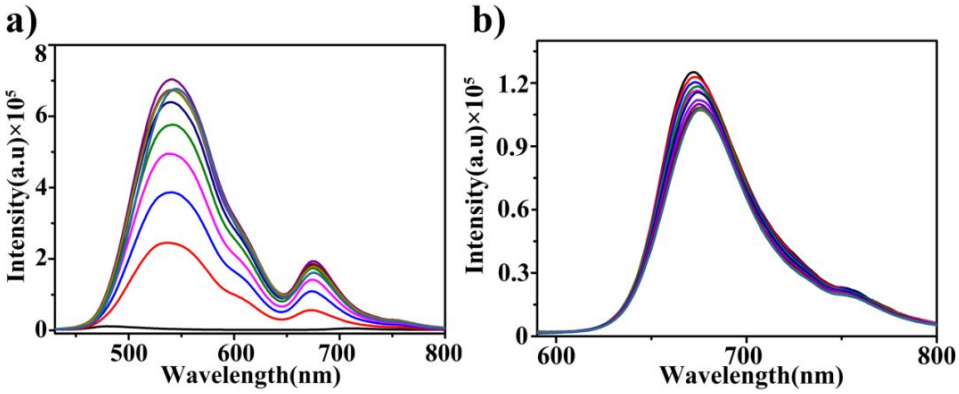

Figure S21. Fluorescence spectra of **R700** (10 μM) titrated with **1**•8Cl^- (0−2.0 equiv) in H_2O. Ex/Em slit = 1.6 nm, (a) λ_{ex} = 410 nm, (b) λ_{ex} = 570 nm.

Energy-transfer efficiency (Φ_{ET})

Energy-transfer efficiency (Φ_{ET}), the fraction of the absorbed energy that is transferred to the acceptor is experimentally measured as a ratio of the fluorescence intensities of the donor in the absence and presence of the acceptor (I_D and I_{DA}). [1]

$$\Phi_{ET} = 1 - I_{DA}/I_D$$

The energy-transfer efficiency(Φ_{ET}) of **1**•8PF_6^- + 2.0 eq. **NiR** ([**1**] = 10 μM) was calculated as 98% at 545 nm in CH_3CN, λ_{ex} = 410 nm, Ex/Em slit = 1.2 nm. The energy-transfer efficiency(Φ_{ET}) of **1**•8Cl^- + 2.0 eq. **R700** ([**1**] = 10 μM) was calculated as 79% at 545 nm in H_2O, λ_{ex} = 410 nm, Ex/Em slit = 1.2 nm. The energy-transfer efficiency(Φ_{ET}) of **1**•8Cl^- + 2.0 eq. **R800** ([**1**] = 10 μM) was calculated as 46.7% at 545 nm in H_2O, λ_{ex} = 410 nm, Ex/Em slit = 1.2 nm.

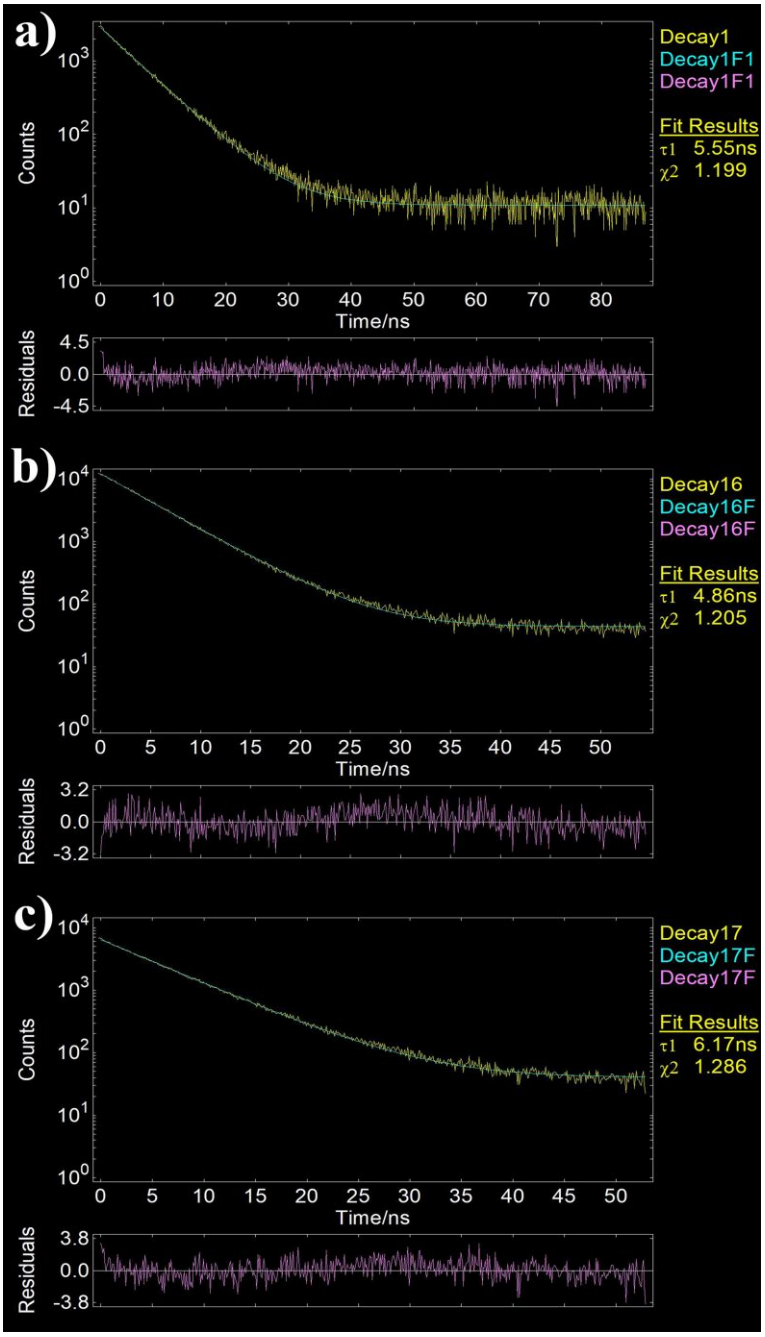

Figure S22. Fluorescence decay profiles of (a) **1**•8PF_6^-, (b) **NiR** and (c) **1**•8PF_6^-□ **NiR** in MeCN.

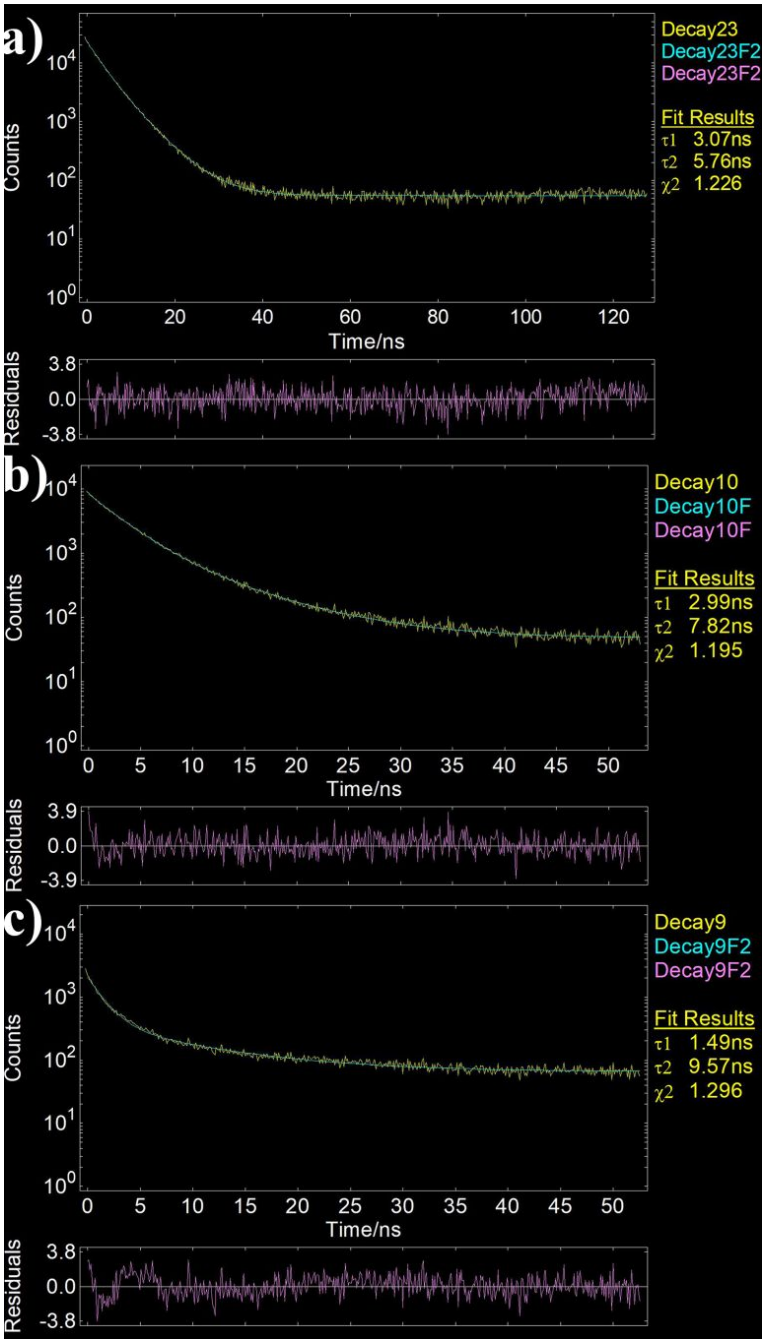

Figure S23. Fluorescence decay profiles of (a) **1**•8Cl^-, (b) **R700** and (c) **1**•8Cl^-□ **R700** in H_2O.

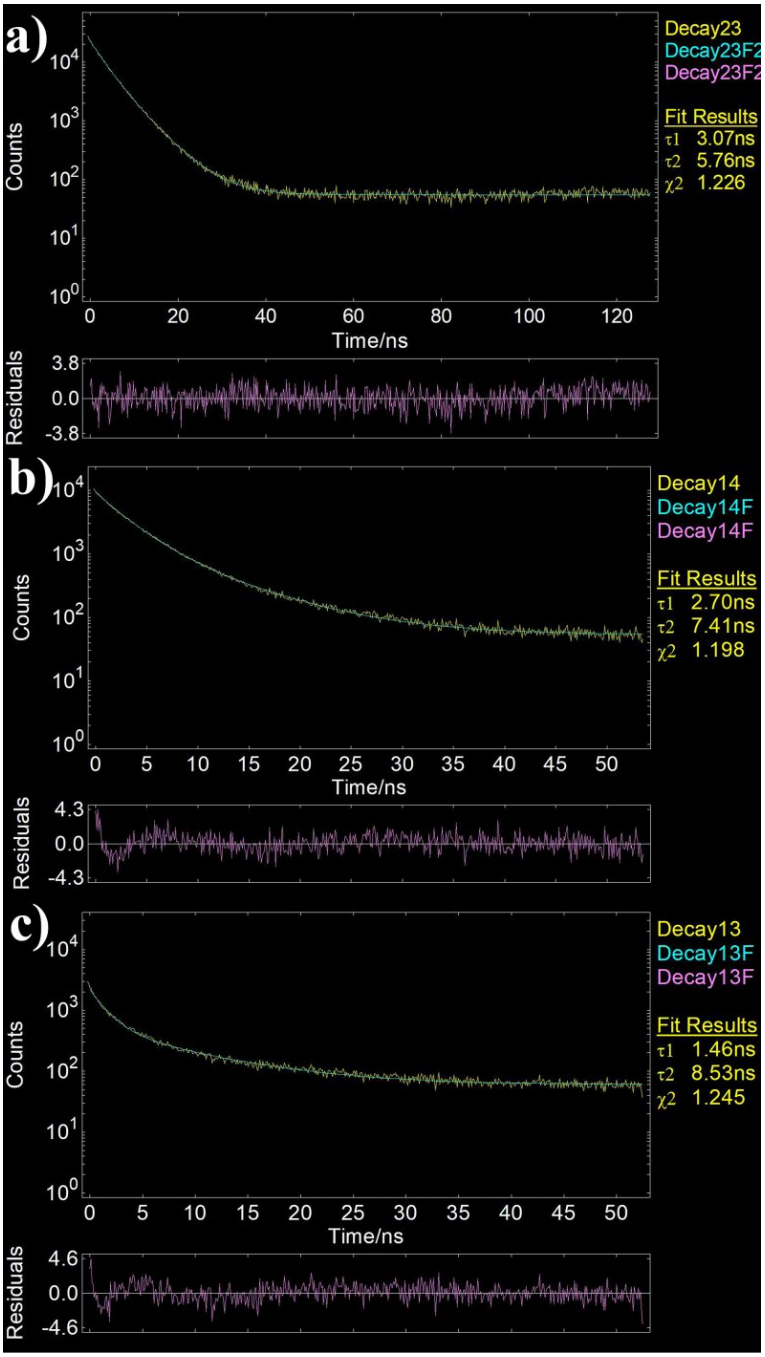

Figure S24. Fluorescence decay profiles of (a) **1**•8Cl$^-$, (b) **R800** and (c) **1**•8Cl$^-$□ **R800** in H_2O.

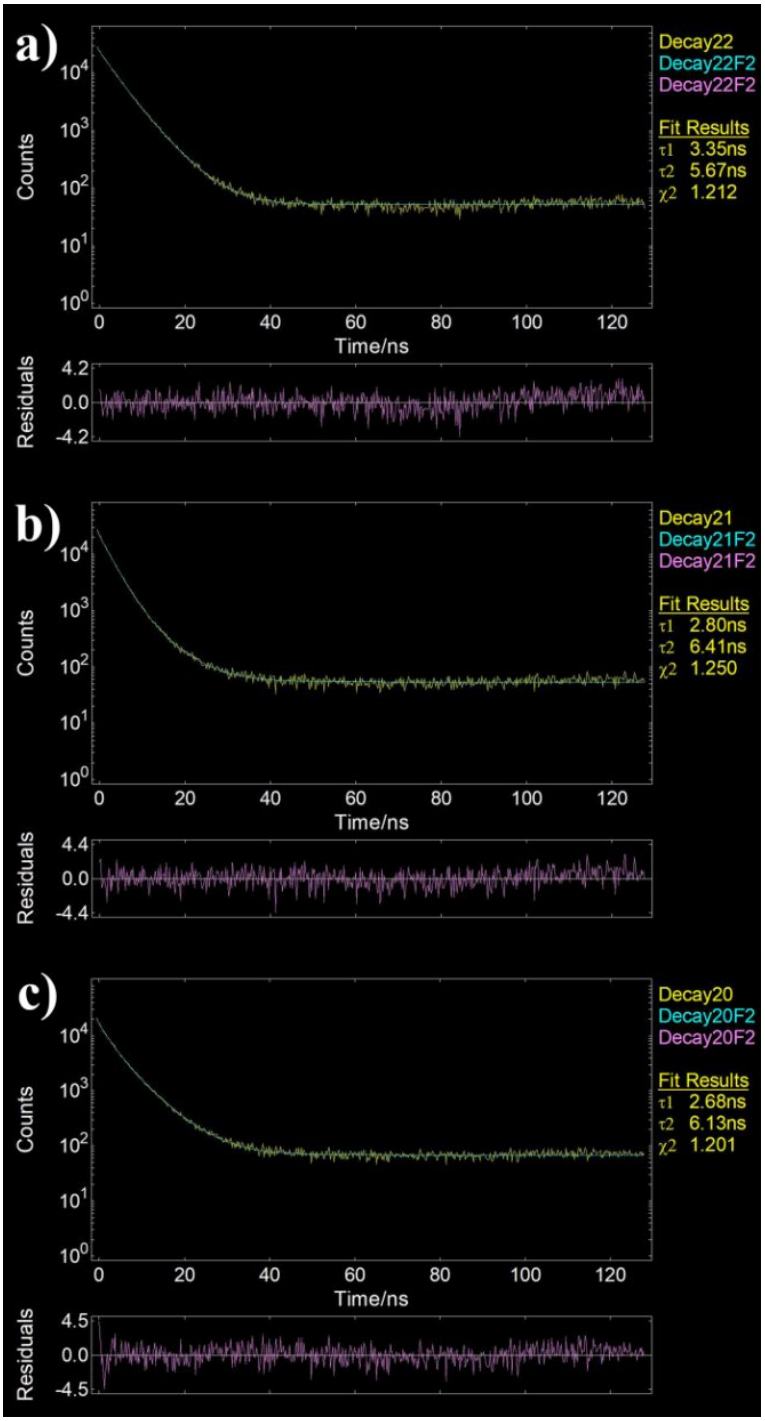

Figure S25. Fluorescence decay profiles of (a) **1**•8Cl⁻⊂**ICG**, (b) **1**•8Cl⁻⊂**AG** and (c) **1**•8Cl⁻⊂**AV** in H_2O.

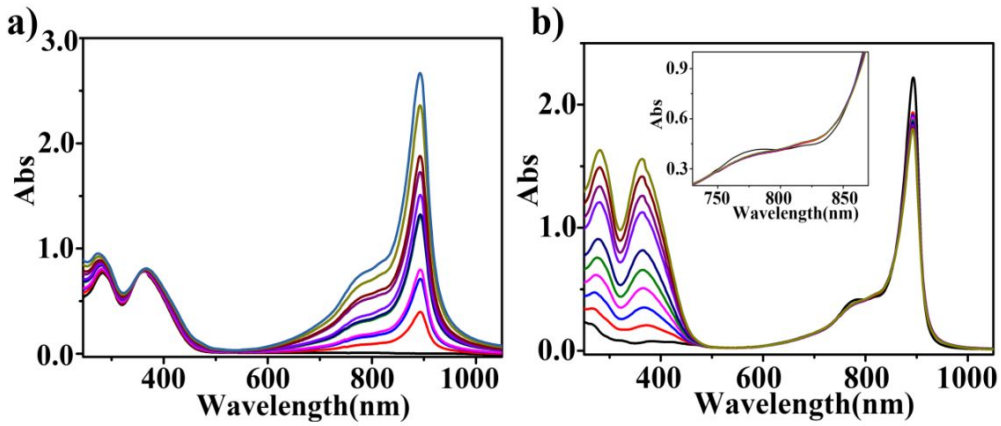

Figure S26. (a) UV/vis spectra of **1**•8Cl$^-$ (10 μM) titrated with **ICG** (0−3.0 equiv) in H_2O. (b) UV/vis spectra of **ICG** (10 μM) titrated with **1**•8Cl$^-$ (0−2.0 equiv) in H_2O.

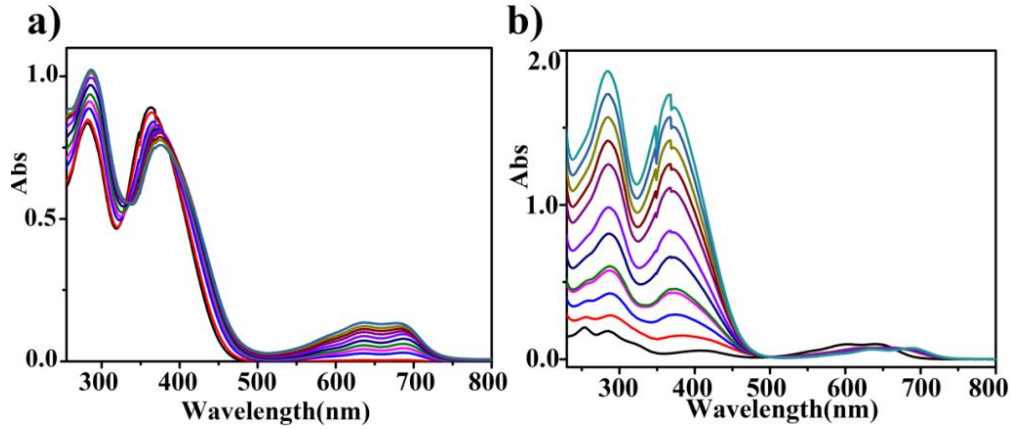

Figure S27. (a) UV/vis spectra of **1**•8Cl$^-$ (10 μM) titrated with **AG** (0−3.0 equiv) in H_2O. (b) UV/vis spectra of **AG** (10 μM) titrated with **1**•8Cl$^-$ (0−2.0 equiv) in H_2O.

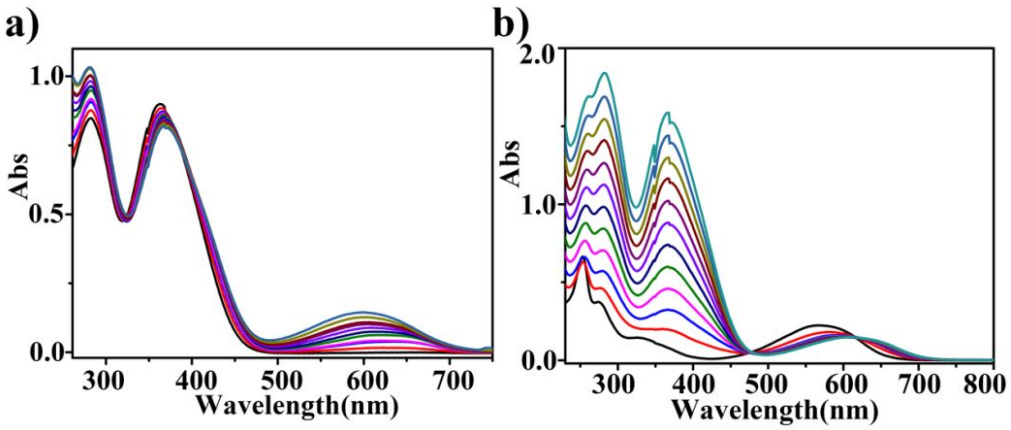

Figure S28. (a) UV/vis spectra of **1**•8Cl$^-$ (10 μM) titrated with **AV** (0−3.0 equiv) in H_2O. (b) UV/vis spectra of **AV** (10 μM) titrated with **1**•8Cl$^-$ (0−2.0 equiv) in H_2O.

The antenna effect under certain concentrations of donor and acceptor equals the ratio of the emission intensity of the acceptor upon excitation of the donor, (λ_{ex} = 410 nm) direct excitation of the acceptor.

$$Antenna\ effect = \frac{I^{(608/678/711)\,nm}_{A+D(\lambda_{ex}=410nm)} - I^{(608/678/711)\,nm}_{D(\lambda_{ex}=410nm)}}{I^{(608/678/711)\,nm}_{A+D(\lambda_{ex}=525/570/620nm)}}$$

The antenna effect of ***1***•*8PF$_6^-$ + 2.0 eq NiR ([1] = 10 μM) was calculated as 81.12 in MeCN. The antenna effect of* ***1***•*8Cl$^-$ + 2.0 eq R700 ([1] = 10 μM) was calculated as 1.30 in H_2O. The antenna effect of* ***1***•*8Cl$^-$ + 2.0 eq R800 ([1] = 10 μM) was calculated as 1.27 in H_2O. When compared with other self-assembled systems, this antenna effect is low.*

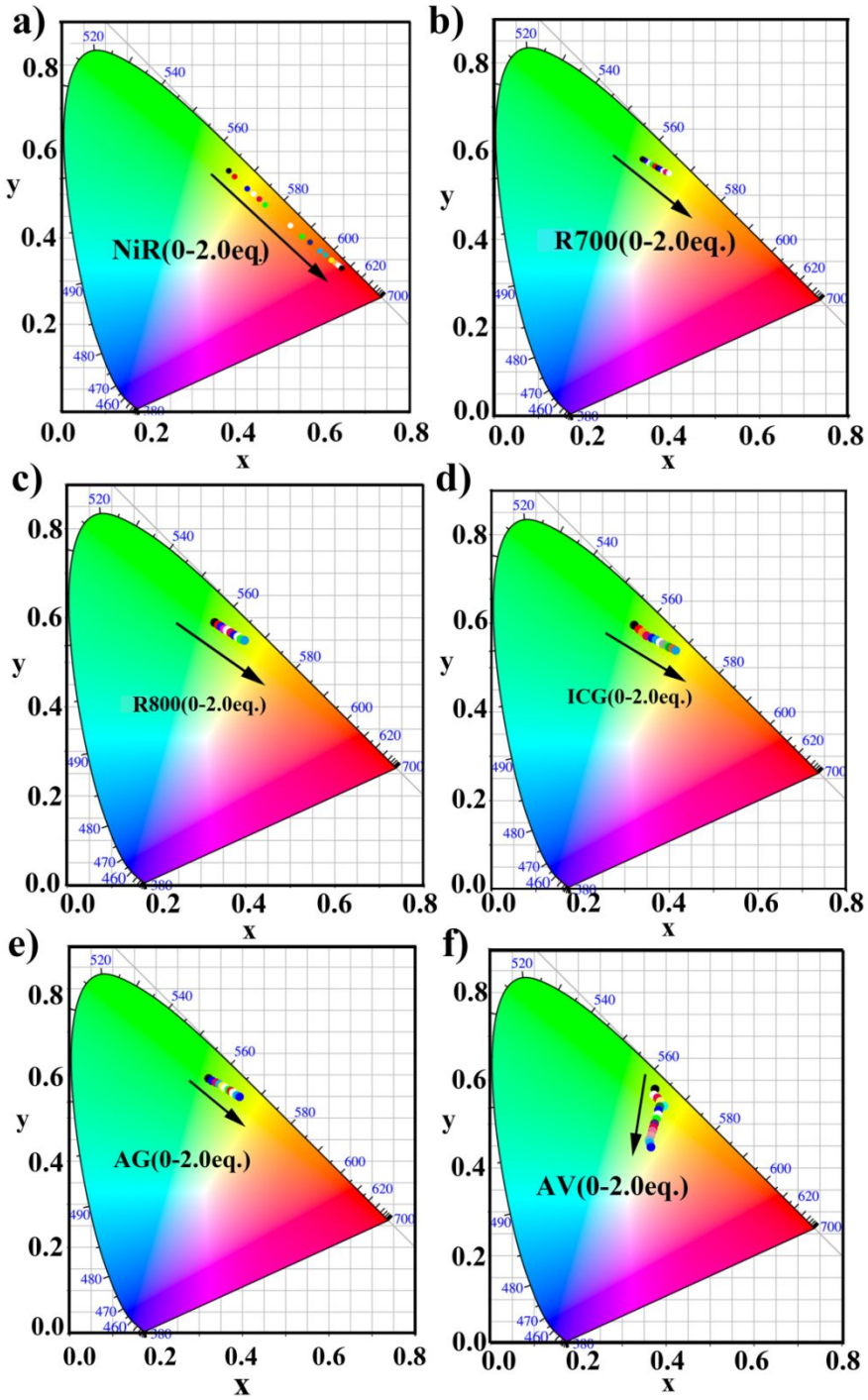

Figure S29. the 1931 CIE chromaticity coordinate changes of **1** (10 μM) titrated with dyes (0−2.0 equiv): (a) **NiR**, (b) **R700**, (c) **R800**, (d) **ICG**, (e) **AG**, (f) **AV**.

Table S2. The redox potentials (vs Ag/AgCl in CH_3CN), HOMO and LUMO Energies of the cages and host-guest complexes.[a]

Compound	ΔE(eV)[b]	$\lambda_{max(onset)}$(nm)	E^1_{Red}/E^2_{Red}(eV)	LUMO/HOMO(eV)[c,d]
1•8PF_6^-	2.71	456.00	-0.70/-1.09	-3.68/-6.39
2•4PF_6^-	2.71	456.00	-0.69/-1.37	-3.69/-6.39
1□NiR	2.66	466.71	-0.48/-0.90	-3.90/-6.56
1□R700	2.65	467.97	-0.65/-0.90	-3.73/-6.38
1□R800	2.64	469.05	-0.59/-0.79	-3.79/-6.43
1□ICG	2.64	468.94	-0.73/-0.96	-3.65/-6.29
1□AG	2.59	479.12	-0.75/-1.14	-3.63/-6.22
1□AV	2.65	468.62	-0.68/-0.90	-3.70/-6.35
NiR	2.07	600.00	-1.16	-3.22/-5.29
R700	1.82	680.70	-0.60/-1.26	-3.78/-5.60
R800	1.68	737.03	-0.60/-1.00	-3.78/-5.46
ICG	1.34	923.25	-0.93	-3.45/-4.79
AG	1.76	705.39	-0.97/-1.29	-3.41/-5.17
AV	1.87	664.13	-0.35/0.97	-4.03/-5.90

[a]Determined by cyclic voltammetry with the ferrocene/ferricenium couple (Fc/Fc+) as external or internal standard. A glassy carbon working electrode, an Ag/AgCl reference electrode and a platinum counter electrode were used to characterize 1.0 mM DMSO solutions of the hexafluorophosphate salts of the analytes at 298 K, with 0.1 M $TBAPF_6$ serving as the supporting electrolyte at a scan rate of 50 mVs^{-1}. Calculation of HOMO and LUMO energies: [b]$\Delta E_{HOMO/LUMO}$ = [1240/($\lambda_{max(onset)}$ (nm)]eV; [c]E_{LUMO} = -[4.8-0.42+E^1_{Red}]eV for E^1_{Red} vs Ag/AgCl; [d]$E_{HOMO} = E_{LUMO}-\Delta E_{HOMO/LUMO}$ eV.

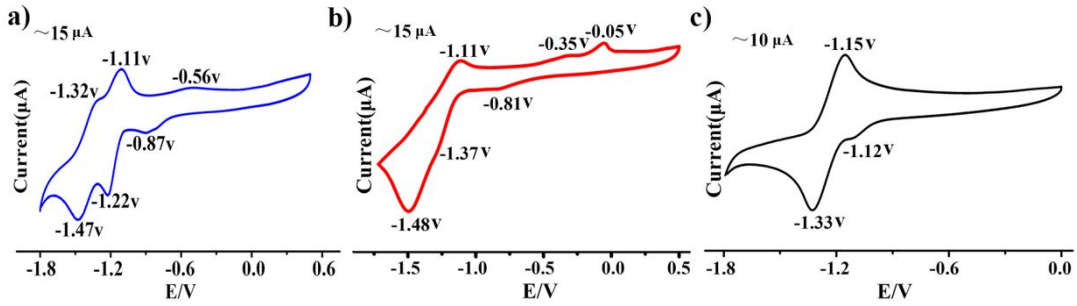

Figure S30. Cyclic voltammetry of (a) **1**•8PF_6^-, (b) **2**•4PF_6^-, (c) **NiR**.

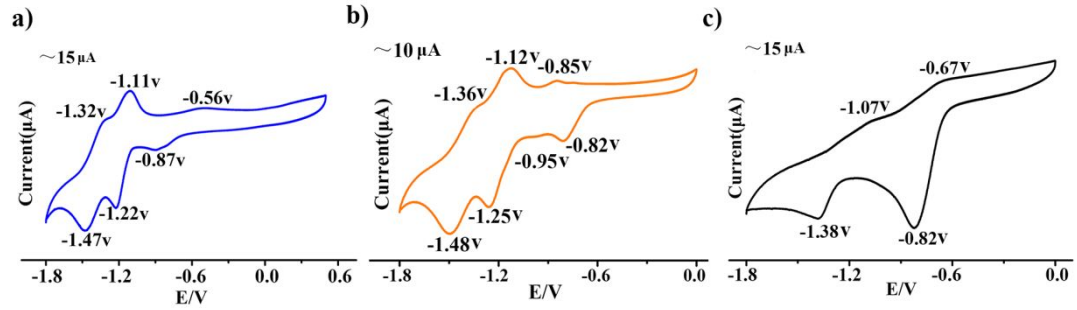

Figure S31. Cyclic voltammetry of (a) **1**•8PF_6^-, (b) **1**•8Cl^-□**R700**, (c) **R700**.

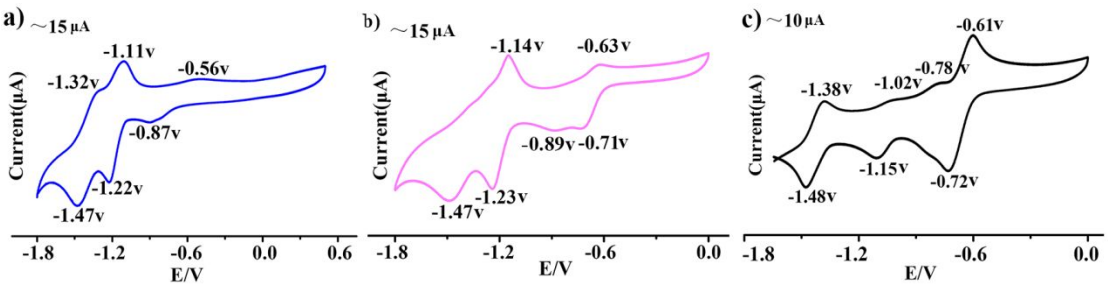

Figure S32. Cyclic voltammetry of (a) **1**•8PF_6^-, (b) **1**•8Cl^-□**R800**, (c) **R800**.

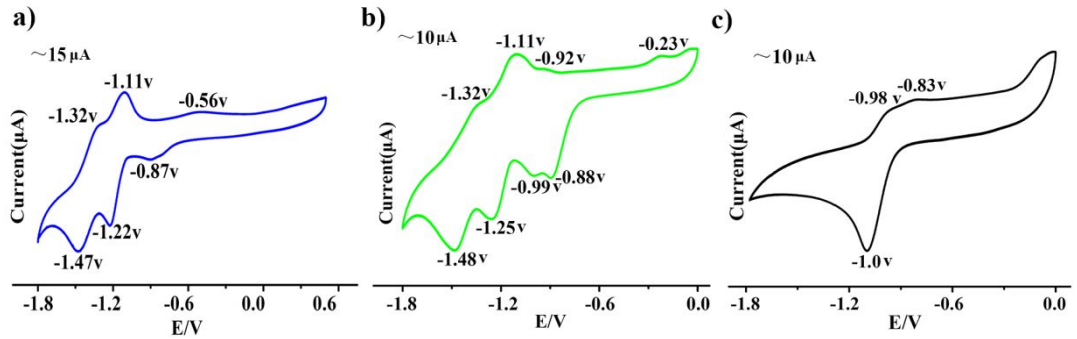

Figure S33. Cyclic voltammetry of (a) **1**•8PF_6^-, (b) **1**•8Cl^-□**ICG**, (c) **ICG**.

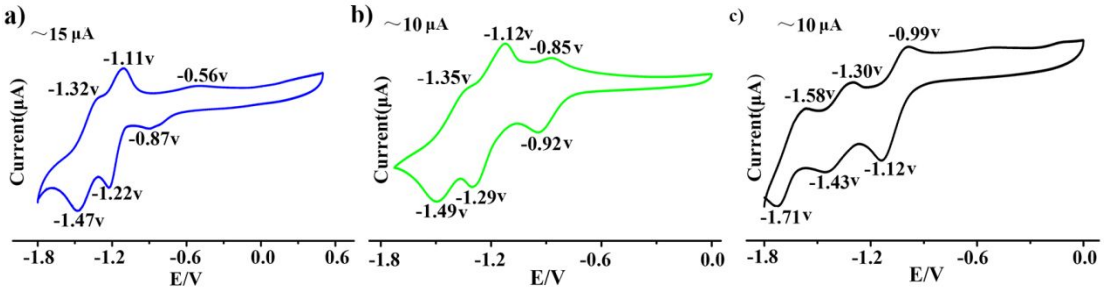

Figure S34. Cyclic voltammetry of (a) **1**•8PF_6^-, (b) **1**•8Cl^-□**AG**, (c) **AG**.

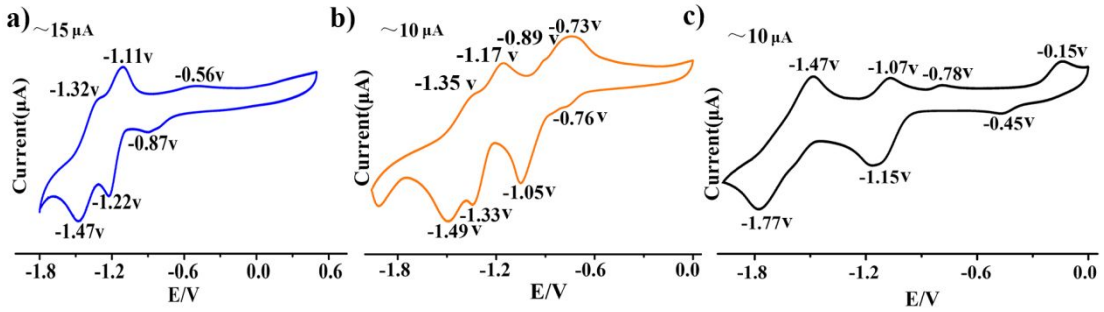

Figure S35. Cyclic voltammetry of (a) **1**•8PF_6^-, (b) **1**•8Cl^-□**AV**, (c) **AV**.

Femtosecond Transient Absorption (fsTA) Experiments.

The fsTA measurements were performed based on a femtosecond Ti:Sapphire regenerative amplified Ti:sapphire laser system (Spectra Physics, Spitfire-Pro) and an automated data acquisition system (Ultrafast Systems, Helios model). The excitation pulse (1 kHz, 240-2,600 nm, pulse width, 120 fs) was generated by an optical parametric amplifier (TOPAS-C, Spectra-Physics) pumped by a regeneratively amplified femtosecond Ti:sapphire laser system (800 nm, 1 kHz, pulse energy 4 mJ, pulse width, 120 fs, Spitfire Pro-F1KXP, Spectra-Physics), which was seeded by a femtosecond Ti-sapphire oscillator (80 MHz, pulse width, 70 fs, 710-920 nm, Maitai XF-1, Spectra-Physics). The probe pulse was obtained by using approximately 5% of the amplified 800 nm output from the Spitfire to generate a white-light continuum (450-800 nm) in a sapphire plate. The maximum extent of the temporal delay was 3300 ps. The instrument response function was determined to be 150 fs. At each temporal delay, data were averaged for 2 s and collected by the acquisition system. The probe beam was split into two before passing through the sample. One probe beam traveled through the sample; the other was sent directly to the reference spectrometer that monitored the fluctuations in the probe beam intensity. Fiber optics was coupled to a multichannel spectrometer with a CMOS sensor that had a 1.5 nm intrinsic resolution. The sample suspension was excited by a 355 nm pump beam. The data were stored as three-dimensional (3D) wavelength-time-absorbance matrices that were exported for use with the fitting software.

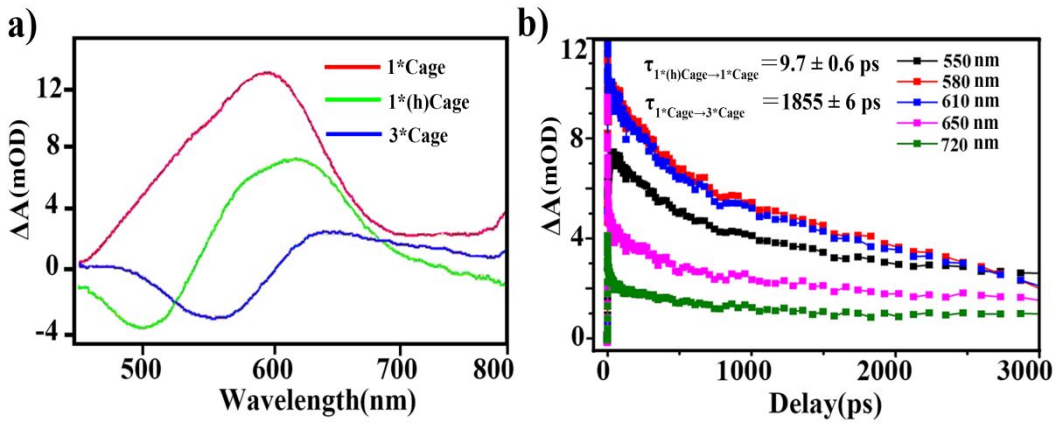

Figure S36. (a) Species-associated spectra obtained from deconvolution of the dataset with the kinetic fit solution. H_2O, λ_{ex} = 355 nm, 1.1 μJ $pulse^{-1}$. (b) Global fits to selected wavelengths in **1**•8Cl^- to the kinetic model described in the text and below.

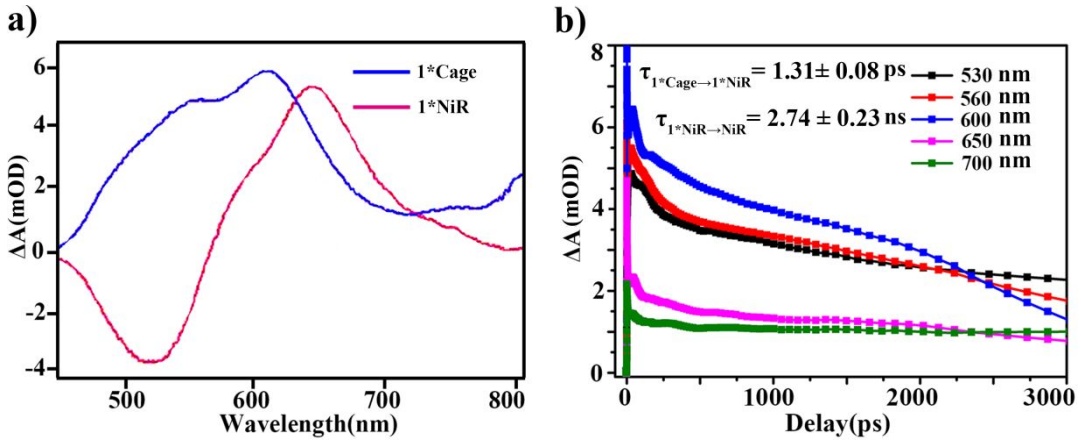

Figure S37. (a) Species-associated spectra obtained from deconvolution of the dataset with the kinetic fit solution. MeCN, λ_{ex} = 355 nm, 1.1 μJ $pulse^{-1}$. (b) Global fits to selected wavelengths in **1**•8PF_6^-□**NiR** to the kinetic model described in the text and below.

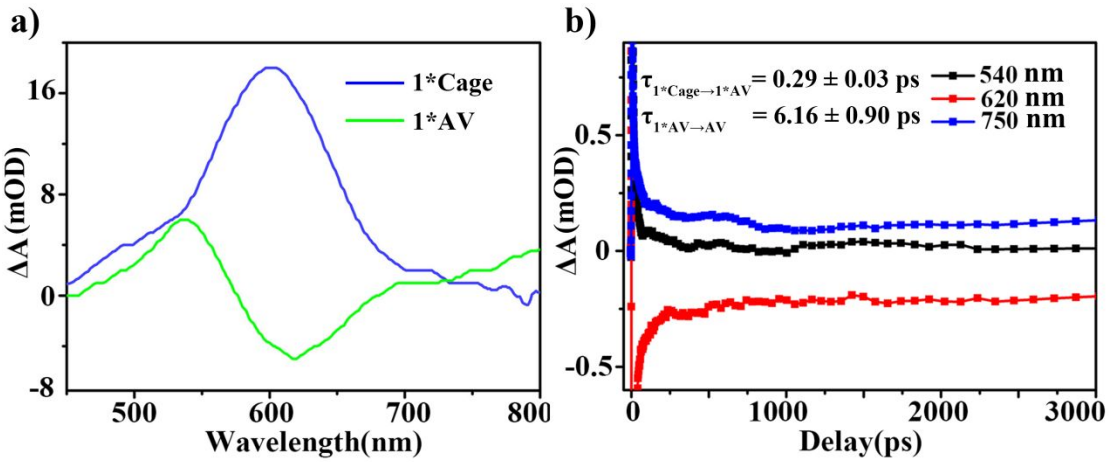

Figure S38. (a) Species-associated spectra obtained from deconvolution of the dataset with the kinetic fit solution. H_2O, λ_{ex} = 355 nm, 1.1 μJ $pulse^{-1}$. (b) Global fits to selected wavelengths in **1**•8Cl^-⊂**AV** to the kinetic model described in the text and below.

Reference

1. H. Duan, Y. Li, Q. Li, P. Wang, X. Liu, L. Cheng, Y. Yu and L. Cao, Fluorescence and Host–Guest Recognition of a Tetraphenylethene-Based Octacationic Cage. *Angew. Chem. Int. Ed.*, **2020**, 59, 10101.

2. Z. Xu, S. Peng, Y. Wang, J. Zhang, A. Lazar, D. Guo, Broad-Spectrum Tunable Photoluminescent Nanomaterials Constructed from A Modular Light-Harvesting Platform Based on Macrocyclic Amphiphiles. *Adv. Mater.* **2016**, *28*, 7666.